

Perturbative renormalization of the Ginzburg–Landau model revisited

J. Kaupužs ^{*}

Institute of Mathematics and Computer Science, University of Latvia
29 Rainja Boulevard, LV-1459 Riga, Latvia

December 21, 2018

Abstract

The perturbative renormalization of the Ginzburg–Landau model is reconsidered based on the Feynman diagram technique. We derive truncated RG flow equations, exactly calculating the vertices appearing in the perturbative renormalization of the φ^4 model up to the ε^3 order of the ε -expansion. The renormalized Hamiltonian contains terms corresponding to different φ^2 , φ^4 , φ^6 , and φ^8 vertices. All these terms are relevant. We have tested the expected basic properties of the renormalization group (RG) flow, such as the semigroup property $R_{s_1 s_2} \mu = R_{s_2} R_{s_1} \mu$, where R_s is the RG operator with scale factor $s > 1$ acting on the set of parameters μ . Besides, the existence of the fixed point and its independence of the parameter s have been verified. All these properties are satisfied, if the RG flow equations are truncated at the order of ε^2 . However, in the next-order calculations, the considered truncation scheme shows no stable fixed point even for the critical parameters of the model. We have tested also a modified approach, where the φ^4 coupling constant u is the expansion parameter at a fixed spatial dimensionality d . In addition to the instability problem, our tests point to an internal inconsistency of such a method.

Keywords: renormalization group, ε -expansion, critical phenomena

^{*}E-mail: kaupuzs@latnet.lv

1 Introduction

The perturbative renormalization of the Ginzburg–Landau (or φ^4) model has a long history (see [1, 2, 3, 4] and references therein). However, as mentioned in [2], a complete formulation of the renormalization group (RG) beyond the ε^2 order of the ε -expansion (where $\varepsilon = 4 - d > 0$, d being the spatial dimensionality) met mathematical difficulties, which could not be overcome. In fact, the ε -expansion of the critical exponents beyond the lowest orders is based on an alternative approach, which relies on the Callan–Symanzik equation [5, 6, 7]. The latter one represents a scaling property of the φ^4 model [5], and the method is based on a set of assumptions [7]. Since the perturbative RG theory is not rigorous, stringent tests of its validity and consistency make sense. Our aim is to perform such tests based on the RG flow equations, truncated in certain way, with the only approximation that the vertices of higher than $\mathcal{O}(\varepsilon^3)$ orders are omitted. In particular, using the Feynman diagram technique, we derive rigorous lower bonds for some of the Hamiltonian parameters in the considered truncation scheme.

We have tested the expected basic properties of the RG flow. Following the idea in [8], we have checked the semigroup property $R_{s_1 s_2} \mu = R_{s_2} R_{s_1} \mu$, where R_s is the RG operator with scale factor $s > 1$ acting on the set of Hamiltonian parameters μ . It is expected that, for the critical parameters of the model, the RG flow converges to certain fixed point μ^* , if the RG transformation R_s is repeated infinitely many times. Besides, the fixed point should be independent of s . We have verified this scenario for the ε -expansion, as well as for an expansion at a fixed spatial dimension d , and have arrived to some interesting and challenging conclusions.

Another strategy of verification has been used in [9], considering a four–dimensional ($d = 4$) model with Gaussian measure modified in such a way to simulate $d = 4 - \varepsilon$ dimensions with ε small and positive. This method allows to control rigorously the remainder of the perturbation series. The obtained results [9] confirm the existence of the non–Gaussian fixed point at a distance $\mathcal{O}(\varepsilon)$ away from the Gaussian one as proposed earlier [1] by the ε -expansion. However, the expected decay of the two–point correlation function appears to be canonical (i. e., Gaussian, see Introduction part in [9]) in disagreement with that provided by the ε -expansion and observed in ordinary spin systems of dimensionality $d < 4$ like, e. g., three–dimensional and two–dimensional Ising models. In view of these observations, the classical (used in the ε -expansion) way of introduction of noninteger spatial dimensionality d via an analytic continuation from d -dimensional hypercubes appears to be more sensible than that in [9]. In fact, there is no unique definition of the noninteger d . It can be introduced in a more physical way as a suitable “fractal” dimension of an irregular lattice [10, 11].

2 Diagrammatic formulation of the renormalization

As a starting point, we consider a φ^4 model with the Hamiltonian H defined by

$$H/T = \int \frac{r}{2} \varphi^2(\mathbf{x}) + \frac{c}{2} (\nabla \varphi(\mathbf{x}))^2 + \frac{1}{8} \int \int \varphi^2(\mathbf{x}_1) u(\mathbf{x}_1 - \mathbf{x}_2) \varphi^2(\mathbf{x}_2) d\mathbf{x}_1 d\mathbf{x}_2 , \quad (1)$$

where the order parameter $\varphi(\mathbf{x})$ is an n -component vector with components $\varphi_i(\mathbf{x})$, depending on the coordinate \mathbf{x} , and T is the temperature. The field $\varphi_j(\mathbf{x})$ is given in Fourier representation by $\varphi_j(\mathbf{x}) = V^{-1/2} \sum_{k < \Lambda} \varphi_{j,k} e^{i\mathbf{k}\mathbf{x}}$, where $V = L^d$ is the volume of the system, d is the spatial dimensionality, and Λ is the upper cutoff of the wave vectors. The Fourier-transformed

Hamiltonian obeys the equation

$$-\frac{H}{T} = -\frac{1}{2} \sum_{i,\mathbf{k}} \left(r + c\mathbf{k}^2 \right) |\varphi_{i,\mathbf{k}}|^2 - \frac{1}{8} V^{-1} \sum_{i,j,\mathbf{k}_1,\mathbf{k}_2,\mathbf{k}_3} \varphi_{i,\mathbf{k}_1} \varphi_{i,\mathbf{k}_2} u_{\mathbf{k}_1+\mathbf{k}_2} \varphi_{j,\mathbf{k}_3} \varphi_{j,-\mathbf{k}_1-\mathbf{k}_2-\mathbf{k}_3} . \quad (2)$$

In the Feynman diagram technique [2, 12], the second term in (2) is represented by a fourth order vertex  (where field components with vanishing total wave vector are related to the solid lines and the remaining factor — to the dashed line). In the following we will consider only a particular case $u(\mathbf{x}) = u\delta(\mathbf{x})$ or $u_{\mathbf{k}} = u$. The fourth order vertex then can be depicted as  by shrinking the dashed line to a point (node). We will mostly use this simplified notation. One has to remember, however, that two of the vertex lines are related to i -th component ($i = 1, \dots, n$), and the other two lines — to j -th component of a field vector (including the possibility $i = j$). It is shown explicitly in the representation  , where these pairs of lines are separated.

In the exact Wilson's RG equation the scale transformation, i. e., the Kadanoff's transformation, is performed by integrating over the Fourier modes with wave vectors obeying $\Lambda/s < k < \Lambda$. It is the first step of the full RG transformation. At this step the transformed Hamiltonian H' is found from the equation

$$e^{-(H'/T) + AL^d} = \int e^{-H/T} \prod_{i, \Lambda/s < k < \Lambda} d\varphi_{i,\mathbf{k}} , \quad (3)$$

where A is a constant. Note that $\varphi_{i,\mathbf{k}}$ is a complex number and $\varphi_{i,-\mathbf{k}} = \varphi_{i,\mathbf{k}}^*$ holds (since $\varphi_i(\mathbf{x})$ is always real), so that the integration over $\varphi_{i,\mathbf{k}}$ in (3) means in fact the integration over real and imaginary parts of $\varphi_{i,\mathbf{k}}$ for each pair of conjugated wave vectors \mathbf{k} and $-\mathbf{k}$. In practice Eq. (3) cannot be solved exactly. It is done perturbatively, as described in [2]. The perturbation terms can be found more easily by means of the Feynman diagrams.

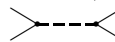
In the perturbative approach, Hamiltonian is split in two parts $H = H_0 + H_1$, where H_0 is the Gaussian part and H_1 is the rest part considered as a small perturbation. The first and the second term on the right hand side of (2) can be identified with $-H_0/T$ and $-H_1/T$, respectively. Since the term with r also is considered as a small perturbation ($r \sim \varepsilon$ holds in the ε -expansion in $d = 4 - \varepsilon$ dimensions), it is suitable to include it in H_1 . In this case diagram expansions are represented by vertices  and  , where the latter second-order vertex corresponds to the term with r .

It is convenient to normalize Eq. (3) by $Z_s = \int \exp(-\tilde{H}_0/T) \prod_{i, \Lambda/s < k < \Lambda} d\varphi_{i,\mathbf{k}}$, where \tilde{H}_0 is the part of H_0 including only the terms with $\Lambda/s < k < \Lambda$. We have $\ln Z_s = A_s L^d$ at $L \rightarrow \infty$, where A_s is independent of L , and the normalization yields

$$-(H'/T) + (A - A_s)L^d = -(H'_0/T) + \ln \langle \exp(-H_1/T) \rangle_0 , \quad (4)$$

where $\langle \cdot \rangle_0$ means the Gaussian average over the field components with $\Lambda/s < k < \Lambda$, whereas H'_0 is the part of H_0 including only the components with $k < \Lambda/s$. Like free energy, $\ln \langle \exp(-H_1/T) \rangle_0$ is represented perturbatively by the sum over all connected Feynman diagrams made of the vertices of $-H_1/T$ by coupling those solid lines, which are associated with wave vectors obeying $\Lambda/s < k < \Lambda$, according to the Wick's theorem. A diagram can contain no coupled lines. There

is also a set of diagrams with all lines coupled. The latter diagrams give a constant (independent of $\varphi_{i,\mathbf{k}}$) contribution which compensates the term $(A - A_s)L^d$ in (4). The other contributions correspond to $-H'/T$.

Each term of $\ln\langle\exp(-H_1/T)\rangle_0$ comes from a diagram (or diagrams) of certain topology and is given by a sum over wave vectors which fulfil certain constraints such that $k < \Lambda/s$ holds for uncoupled (external or outer) solid lines, associated with field components $\varphi_{i,\mathbf{k}}$, and $\Lambda/s < k < \Lambda$ holds for coupled solid lines. Besides, the sum of all wave vectors coming into any of the nodes is zero, and the same index i is related to the solid lines attached to one node of any vertex  or . The Gaussian average $G_0(\mathbf{k}) = \langle \varphi_{i,\mathbf{k}} \varphi_{i,-\mathbf{k}} \rangle_0 = \langle |\varphi_{i,\mathbf{k}}|^2 \rangle_0$ is related to a coupling line with wave vector \mathbf{k} . Here $G_0(\mathbf{k})$ is the Fourier transform of the two-point correlation function in the Gaussian approximation. If only the term with \mathbf{k}^2 in (2) is included in H_0/T , then we have $G_0(\mathbf{k}) = 1/(ck^2)$. Including also the term with r , we have $G_0(\mathbf{k}) = 1/(r + ck^2)$, but in this case we need finally to expand $G_0(\mathbf{k})$ in terms of r . The second method yields the same results as the first one: such an expansion generates the same terms, which are obtained in the first method by extending coupling lines in the diagrams originally constructed without vertices  to include all possible linear chains made of these vertices. We will use the first, i. e., more diagrammatic method. Note that, when the renormalization procedure is repeated, a continuum of additional vertices appear in the expansion of $-H_1/T$, including ones with explicit wave-vector dependent factors related to the solid lines, which then also have to be taken into account.

In fact, the first step of RG transformation implies the summation over wave vectors of the coupled lines in the diagrams, resulting in a Hamiltonian which depends on $\varphi_{i,\mathbf{k}}$ with $k < \Lambda/s$. The RG transformation has the second step [2]: changing of variables $\tilde{\mathbf{k}} = s\mathbf{k}$ and rescaling the field components $\varphi_{i,\mathbf{k}} \rightarrow s^{1-\eta/2}\varphi_{i,\tilde{\mathbf{k}}}$, where η is the critical exponent describing the $\sim k^{-2+\eta}$ singularity of the Fourier-transformed critical two-point correlation function at $k \rightarrow 0$. The upper cutoff for the new wave vectors $\tilde{\mathbf{k}}$ is the original one Λ , whereas the density of points in the $\tilde{\mathbf{k}}$ -space corresponds to s^d times decreased volume. Therefore we make a substitution $\tilde{V} = s^{-d}V$. In the thermodynamic limit we can replace \tilde{V} by V consistently increasing the density of points in the wave vector space. Finally, we set $\tilde{\mathbf{k}} \rightarrow \mathbf{k}$ and obtain a Hamiltonian in original notations.

3 Renormalization up to the order of ε^2

3.1 RG flow equations

Here we consider RG flow equations including all terms up to the order $\mathcal{O}(\varepsilon^2)$, starting with the renormalization of the coupling constant u . In fact, this is the lowest order of the theory, since it allows to find the fixed point value u^* up to the order of ε . Our aim is to show that we can easily recover the known results using the diagrammatic approach described in Sec. 2. It allows also to write down unambiguously (i. e., without intermediate approximations) the formulae for all perturbation terms.

Important statements here are that the renormalized values of r and u are quantities of order $\mathcal{O}(\varepsilon)$. Besides, $\eta = \mathcal{O}(\varepsilon^2)$ holds within the ε -expansion and, for any finite renormalization scale s , the variation of c is of order $\mathcal{O}(\varepsilon^2)$ [2]. Hence, performing the RG transformation R_s with a finite s , the only diagrams of $\ln\langle\exp(-H_1/T)\rangle_0$ contributing to the renormalized coupling constant up to the order of ε^2 are  and  (this statement can be verified in detail based on a complete renormalization discussed further on). The first one provides the

original φ^4 term in Eq. (2), which is merely renormalized by factor $s^{\varepsilon-2\eta}$ at the second step of the RG transformation. The second diagram, which is constructed of two vertices  , yields

$$\begin{aligned} \text{Diagram} &\rightarrow s^{\varepsilon-2\eta} \left(\frac{u}{8c} \right)^2 V^{-1} \sum_{i,j,\mathbf{k}_1,\mathbf{k}_2,\mathbf{k}_3} \varphi_{i,\mathbf{k}_1} \varphi_{i,\mathbf{k}_2} \varphi_{j,\mathbf{k}_3} \varphi_{j,-\mathbf{k}_1-\mathbf{k}_2-\mathbf{k}_3} \times \\ &\times [(4n+16) Q((\mathbf{k}_1 + \mathbf{k}_2)/s, s) + 16 Q((\mathbf{k}_1 + \mathbf{k}_3)/s, s)] . \end{aligned} \quad (5)$$

Here Q is given by

$$Q(\mathbf{k}, s) = \frac{1}{(2\pi)^d} \int_{\Lambda/s < q < \Lambda} q^{-2} |\mathbf{k} - \mathbf{q}|^{-2} \mathcal{F}(|\mathbf{k} - \mathbf{q}|, s) d^d q , \quad (6)$$

where $\mathcal{F}(k, s) = 1$ if $\Lambda/s < k < \Lambda$, and $\mathcal{F}(k, s) = 0$ otherwise. To obtain this result, we have deciphered the  diagram as a sum of three diagrams of different topologies made of vertices  , i. e.,  ,  , and  , providing the same topological picture  when shrinking the dashed lines to points. Note that any loop made of solid lines of  gives a factor n , and one needs also to compute the combinatorial factors (see, e. g., [2, 12]). For the above three diagrams, the resulting factors are 4n, 16, and 16, which enter the prefactors of Q in (5).

Quantity $Q(\mathbf{k}/s, s)$ has a constant contribution

$$Q(\mathbf{0}, s) = K_d \Lambda^{-\varepsilon} (s^\varepsilon - 1)/\varepsilon , \quad (7)$$

as well as a \mathbf{k} -dependent correction $\Delta(k, s) = Q(\mathbf{k}/s, s) - Q(\mathbf{0}, s)$ vanishing at $k = 0$. Here $K_d = S(d)/(2\pi)^d$, where $S(d) = 2\pi^{d/2}/\Gamma(d/2)$ is the area of unit sphere in d dimensions.

The term provided by the $Q(\mathbf{0}, s)$ part of $Q(\mathbf{k}/s, s)$ in (5) is identified with the φ^4 vertex, contributing to the renormalized coupling constant u' . It is consistent with the general form

$$V^{-1} \sum_{i,j,\mathbf{k}_1,\mathbf{k}_2,\mathbf{k}_3} \bar{Q}(\mathbf{k}_1, \mathbf{k}_2, \mathbf{k}_3, s, n, \varepsilon) \varphi_{i,\mathbf{k}_1} \varphi_{i,\mathbf{k}_2} \varphi_{j,\mathbf{k}_3} \varphi_{j,-\mathbf{k}_1-\mathbf{k}_2-\mathbf{k}_3} , \quad (8)$$

of quartic (φ^4) terms, where the contribution corresponding to the ordinary φ^4 vertex is uniquely identified with one provided by the constant part $\bar{Q}(\mathbf{0}, \mathbf{0}, \mathbf{0}, s, n, \varepsilon)$ of the weight function \bar{Q} .

Taking into account also the contribution coming directly from  vertex, the RG flow equation reads

$$u' = s^{\varepsilon-2\eta} \left[u - u^2 \frac{K_d(n+8)}{2c^2\Lambda^\varepsilon} \times \frac{s^\varepsilon - 1}{\varepsilon} \right] + \mathcal{O}(\varepsilon^3) , \quad (9)$$

where u' is the renormalized and u is the original coupling constant. The expansion in ε yields the well known equation [2]

$$u' = u + \varepsilon u \ln s - u^2 B \ln s + \mathcal{O}(\varepsilon^3) , \quad (10)$$

where $B = K_4(n+8)/(2c^2)$, with the known fixed-point value at $u = u^* = B^{-1}\varepsilon + \mathcal{O}(\varepsilon^2)$.

The correction term $\Delta(k, s)$ changes the renormalized Hamiltonian as follows:

$$\begin{aligned} H/T &\rightarrow (H/T) - s^{\varepsilon-2\eta} \left(\frac{u}{2c} \right)^2 V^{-1} \sum_{i,j,\mathbf{k}_1,\mathbf{k}_2,\mathbf{k}_3} \varphi_{i,\mathbf{k}_1} \varphi_{i,\mathbf{k}_2} \varphi_{j,\mathbf{k}_3} \varphi_{j,-\mathbf{k}_1-\mathbf{k}_2-\mathbf{k}_3} \times \\ &\times [(1+n/4) \Delta(|\mathbf{k}_1 + \mathbf{k}_2|, s) + \Delta(|\mathbf{k}_1 + \mathbf{k}_3|, s)] . \end{aligned} \quad (11)$$

It can be represented as a sum of two fourth-order vertices including prefactors $\Delta(|\mathbf{k}_1 + \mathbf{k}_2|, s)$ and $\Delta(|\mathbf{k}_1 + \mathbf{k}_3|, s)$, respectively, related to two of the vertex lines.

In the following we will introduce a more suitable diagrammatic notation. In the one-component case $n = 1$, the term appearing in (5) is represented as

$$s^{2\varepsilon-2\eta} \frac{9}{16} u^2 \text{--->---<} \quad (12)$$

where --->---< is the Feynman diagram in which the Gaussian propagator $1/(ck^2)$ with $k \in [\Lambda, s\Lambda]$ is related to the dotted coupling lines. In other words, the propagator is multiplied with the cut function $\mathcal{F}(k/s, s)$. In general (also for other diagrams considered in our paper), the field components supplied with the factor V^{1-m} are related to $2m$ external lines, the rest of such factors being absorbed in the \mathbf{k} -space integrals. An additional s^ε factor in (12) comes from the rescaling of wave vectors in such a way that the integration now takes place over $k \in [\Lambda, \Lambda s]$ for the internal lines. This procedure is necessary in order to represent the result as a Feynman diagram with vanishing sum of the wave vectors entering each node.

Subtracting from the \mathbf{k} -space integral its value calculated at $\mathbf{k} = \mathbf{0}$ for the external lines, the result is represented as

$$s^{2\varepsilon-2\eta} \frac{9}{16} u^2 \text{--->---< } . \quad (13)$$

Similar notation is applied throughout the paper, where the line crossing the diagram indicates the subtraction of zero- \mathbf{k} contribution. The diagram representation of this kind has been proposed in [13]. In the general n -component case, we denote by

$$\Sigma \left(\text{--->---<} \right) = \frac{n}{9} \text{--->---<} + \frac{4}{9} \text{--->---<} \text{--->---<} + \frac{4}{9} \text{--->---<} \text{--->---<} \quad (14)$$

the sum of all such kind of diagrams, which reduce to --->---< when the dashed lines shrink to points. In (14) the coefficients are normalized in such a way that their sum is 1 at $n = 1$. Note that in the diagram technique with such vertices, one has to count closed loops made of all kind of lines related to the propagator $1/(ck^2)$. In this notation (11) becomes

$$H/T \rightarrow (H/T) - s^{2\varepsilon-2\eta} u^2 \frac{9}{16} \Sigma \left(\text{--->---<} \right) \quad (15)$$

Analogous diagrammatic representation is possible for all vertices appearing in a repeated renormalization. In accordance with such notation, the ordinary φ^4 vertex in (2) will be represented as $-(u/8) \text{--->---<}$.

For a complete renormalization up to the order of ε^2 , one has to take into account also other contributions of this order, including the φ^6 vertex

$$\begin{aligned} \Sigma \left(\text{--->---<} \right) &\equiv \text{--->---<} \\ &= c^{-1} V^{-2} \sum_{i,j,l,\mathbf{k}_1,\mathbf{k}_2,\mathbf{k}_3,\mathbf{k}_4,\mathbf{k}_5} \varphi_{i,\mathbf{k}_1} \varphi_{i,\mathbf{k}_2} \varphi_{j,\mathbf{k}_3} \varphi_{j,\mathbf{k}_4} \varphi_{l,\mathbf{k}_5} \varphi_{l,-\mathbf{k}_1-\mathbf{k}_2-\mathbf{k}_3-\mathbf{k}_4-\mathbf{k}_5} \\ &\quad \times |\mathbf{k}_1 + \mathbf{k}_2 + \mathbf{k}_3|^{-2} \mathcal{F}(|\mathbf{k}_1 + \mathbf{k}_2 + \mathbf{k}_3|/s, s) \end{aligned} \quad (16)$$

appearing due to the coupling of two vertices --->---< , as well as the quadratic term of the general form $(1/2) \sum_{i,\mathbf{k}} \tilde{\theta}(\mathbf{k}) |\varphi_{i,\mathbf{k}}|^2$ provided by diagrams with two external lines. In the representation $\tilde{\theta}(\mathbf{k}) = r + c\mathbf{k}^2 + \theta(\mathbf{k})$, it corresponds to the φ^2 vertex in (2) with one additional term.

In the rest part of this section we will consider the structure of the renormalized Hamiltonian and the related RG flow equations, providing the proofs afterwards in Sec. 3.2. Thus, the renormalized Hamiltonian has the form

$$\begin{aligned} \frac{H}{T} &= \frac{1}{2} \sum_{i,\mathbf{k}} \left(r + c\mathbf{k}^2 + \theta(\mathbf{k}) \right) |\varphi_{i,\mathbf{k}}|^2 + \frac{u}{8} \times \text{---} \times \\ &+ a_4 \Sigma \left(\text{---} \times \text{---} \times \right) + a_6 \Sigma \left(\text{---} \dots \text{---} \times \right) + \mathcal{O}(\varepsilon^3) . \end{aligned} \quad (17)$$

Here the wave vectors of the dotted lines are in the interval $[\Lambda, \zeta\Lambda]$, where the parameter ζ has the initial value 1 and is transformed according to

$$\zeta' = s \zeta \quad (18)$$

in a process of repeated renormalization. Here ζ is the previous and ζ' is the new (renormalized) value of this parameter after the current RG transformation (RGT) with the scale factor s . The weight coefficients a_4 and a_6 in this order of the ε -expansion obey simple RG flow equations

$$a'_4 = -\frac{9u^2}{16} + \mathcal{O}(\varepsilon^3) \quad (19)$$

$$a'_6 = -\frac{u^2}{8} + \mathcal{O}(\varepsilon^3) \quad (20)$$

relating the new values of these parameters in each RGT to the previous value of u . The initial values of a_4 and a_6 are not important, since the corresponding diagrams vanish at $\zeta = 1$. The RG flow equations for the Hamiltonian parameters u and r read

$$r' = s^2 \left(r + \frac{n+2}{2} u \mathbf{0} \bullet \bigcirc - \frac{n+2}{2} r u \mathbf{0} \bigcirclearrowleft - \left(\frac{n+2}{2} \right)^2 u^2 \mathbf{0} \bigcirclearrowleft \times \mathbf{0} \bullet \bigcirc \right. \\ \left. + \frac{n+2}{2} \left[-u^2 \mathbf{0} \bigcirclearrowright + \frac{16}{3} a_4 D_1 \left(\frac{\Lambda}{s}, \Lambda, \zeta \Lambda \right) + 24 a_6 D_2 \left(\frac{\Lambda}{s}, \Lambda, \zeta \Lambda \right) \right] \right) + \mathcal{O}(\varepsilon^3), \quad (22)$$

where  is the diagram with amputated four external lines having zero wave vectors, those of the internal solid lines being in the range $[\Lambda/s, \Lambda]$. The other diagrams here are defined analogously, whereas the quantities D_1 and D_2 are given by

$$D_1(\Lambda_1, \Lambda_2, \Lambda_3) = 0 \circlearrowleft - 0 \circlearrowright \times 0 \circlearrowright \circlearrowleft , \quad (23)$$

where the wave vectors of the solid lines are within $[\Lambda_1, \Lambda_2]$, and those of the dotted lines — within $[\Lambda_2, \Lambda_3]$. Eq. (21) is the same as (9), only the irrelevant for this order of the ε -expansion factor $s^{-2\eta}$ is omitted, like also the factor $s^{-\eta}$ in (22).

The parameter c enters all diagrams. In the actual order of the ε -expansion its variation does not produce additional terms in (21) and (22). However, one has to update its value according to the equation

$$c' = s^{-\eta} \left(c - \frac{n+2}{2} \Pi \right) + \mathcal{O}(\varepsilon^3) , \quad (25)$$

where

$$\Pi = \lim_{k \rightarrow 0} \frac{D(k) - D(0)}{k^2} . \quad (26)$$

Here

$$D(k) = u^2 \left\{ \text{ k } \bigcirc \bigcirc \right\} - \frac{16}{3} a_4 \left\{ \text{ k } \bigcirc \bigcirc \bigcirc \right\} - 24 a_6 \left\{ \text{ k } \bigcirc \bigcirc \bigcirc \bigcirc \right\} , \quad (27)$$

were $k \in [\Lambda/s, \Lambda]$ corresponds to the solid lines and $k \in [\Lambda, \Lambda\zeta]$ — to the dotted lines in the diagrams, whereas the symbol \mathbf{k} indicates the wave vector related to the amputated external line. Finally, the RG flow equation for the function $\theta(\mathbf{k})$ reads

$$\theta'(\mathbf{k}) = s^2 \left(\theta(\mathbf{k}/s) - \frac{n+2}{2} \Phi(\mathbf{k}/s) \right) + \mathcal{O}(\varepsilon^3) , \quad (28)$$

where

$$\Phi(\mathbf{k}) = D(k) - D(0) - k^2 \Pi . \quad (29)$$

Using the diagram technique, the function $\theta(\mathbf{k})$ can be represented as

$$\theta(\mathbf{k}) = -\frac{n+2}{2} u^2 \text{ k } \bigcirc \bigcirc \bigcirc \bigcirc + \mathcal{O}(\varepsilon^3) , \quad (30)$$

where the wavy line indicates that both the constant contribution and that proportional to k^2 (with the proportionality coefficient determined at $k \rightarrow 0$) are subtracted. Besides, the range of the wave vectors for the internal lines is $[\Lambda, \Lambda\zeta]$, where ζ is determined after the actual RGT.

3.2 Proof of the RG flow equations

In Sec. 3.1 the RG flow equations are given without proof. Their proof consists of a verification that, at each RGT, the Hamiltonian keeps the form (17) in accordance with the given update rules for all parameters. Consider first the φ^6 vertex at $n = 1$, summing up all diagrams of this topology, which appear in H/T at a given RGT:

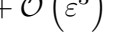
$$\begin{aligned} s^{2\varepsilon-3\eta} \left(-\frac{u^2}{8} \text{ } \nearrow \text{ } \nwarrow + a_6 \text{ } \nearrow \text{ } \text{---} \text{ } \nwarrow \right) &= -\frac{u^2}{8} \left(\text{ } \nearrow \text{ } \nwarrow + \text{ } \nearrow \text{ } \text{---} \text{ } \nwarrow \right) + \mathcal{O}(\varepsilon^3) \\ &= -\frac{u^2}{8} \text{ } \nearrow \text{ } \text{---} \text{ } \nwarrow + \mathcal{O}(\varepsilon^3) = a'_6 \text{ } \nearrow \text{ } \text{---} \text{ } \nwarrow + \mathcal{O}(\varepsilon^3) . \end{aligned} \quad (31)$$

Here the wave vectors within $[\Lambda, \Lambda s]$, $[\Lambda s, \Lambda \zeta']$, and $[\Lambda, \Lambda \zeta']$ correspond to the solid, dashed, and dotted coupling lines, respectively, where $\zeta' = s\zeta$. (These dashed lines should not be confused with those of $\text{ } \nearrow \text{ } \text{---} \text{ } \nwarrow$.) In (31), the vertex $\text{ } \nearrow \text{ } \nwarrow$ is produced by coupling (and rescaling) two φ^4 vertices $\text{ } \times \text{ } \times$, whereas $\text{ } \nearrow \text{ } \text{---} \text{ } \nwarrow$ comes from the rescaling of already existing before the given RGT φ^6 vertex. Apart from other approximations, we have omitted the irrelevant for this order of the ε -expansion rescaling factor resulting from the renormalization of parameter c . We have used the substitution $a_6 = -u^2/8 + \mathcal{O}(\varepsilon^3)$, which holds according to the assumption that our RG flow equation (20) was satisfied and u was changed only by $\mathcal{O}(\varepsilon^2)$ in the previous RGT. It is true for the first RGT, so that the relations (31) provide the proof of (20) by induction. It is obviously valid for any finite number of RGT.

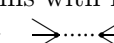
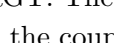
The generalisation to the n -component case is trivial here, since there is only one way how to couple two vertices $\text{ } \nearrow \text{ } \text{---} \text{ } \nwarrow$ to form the sixth-order vertex.

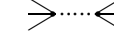
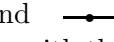
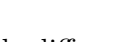
Similarly, the summation of terms provided by the diagrams of  topology, subtracting the contribution included in the ordinary φ^4 vertex, gives us

$$\begin{aligned}
& s^{2\varepsilon-2\eta} \left(-\frac{9u^2}{16} \times \times + a_4 \times \times \times + 9a_6 \times \times \times \right) \\
& = -\frac{9u^2}{16} (\times \times + \times \times \times + 2 \times \times \times) + \mathcal{O}(\varepsilon^3) \\
& = -\frac{9u^2}{16} \times \times \times + \mathcal{O}(\varepsilon^3) = a'_4 \times \times \times + \mathcal{O}(\varepsilon^3)
\end{aligned} \tag{32}$$

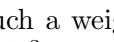
with the same k intervals for different coupling lines as in (31). It proves (19) for a finite number m of RG transformations at $n = 1$. Here the three diagrams in the first line of (32) come from two  vertices, rescaling of the already existing vertex with the coefficient a_4 , and from the φ^6 vertex via coupling its two lines. Besides,  \equiv  holds, since the diagram  vanishes if the external lines have zero wave vectors. This derivation is easily generalised to the n -component case represented by (17): the same relations, only multiplied with the corresponding weight factors in (14), hold for diagrams of each topology, when  is deciphered as the diagrams on the right hand side of (14).

A subtle question here is whether the small corrections, omitted in (31) and (32) at each RGT, do not lead to larger than $\mathcal{O}(\varepsilon^3)$ deviations from the assumed form of the renormalized Hamiltonian when the number of RG transformations m growth unlimitedly. A rigorous answer to this question can be found, comparing the results of the actual update rules with those provided by a renormalization scheme in which all these corrections are taken into account. Such a scheme will be considered in Sec. 4. Here we note only that the actual RG flow equations are valid within the given accuracy for any m .

The derivation of (21) has been already discussed in Sec. 3.1. Recall that the updated value of the coupling constant u of the ordinary φ^4 vertex is related to the constant part of the weight function in (8), which comes from the rescaled already existing ordinary φ^4 vertex, as well as from other diagrams with four external lines generated in the actual RGT. The coupling of two lines of the vertex  gives vanishing contribution here, so that the coupling  is the only relevant one at the order of ε^2 . It results in (21).

Similarly, the updated value of the parameter r is identified with the constant part of the weight function $\tilde{\theta}(\mathbf{k})$ in the general representation of the quadratic term $(1/2) \sum_{i,\mathbf{k}} \tilde{\theta}(\mathbf{k}) |\varphi_{i,\mathbf{k}}|^2$, and is generated by the diagrams with two external lines. It results in (22), where the terms with a_4 and a_6 appear via coupling the lines of the vertices  and  , respectively, whereas other diagrams in (22) are produced by the vertices  and  .

The RG flow equation (25) for the parameter c is similar to that for r with the only difference that here we single out the contribution to $\tilde{\theta}(\mathbf{k})$, which is proportional to k^2 . Subtracting both the constant contribution and that of k^2 , we arrive to the equation for $\theta(\mathbf{k})$ (28). Its diagrammatic form (30) is proven by summation of diagrams like, e. g., in Eq. (32).

Finally, we check that all terms up to the order of ε^2 are already included. In particular, the part of (17) with factor $\theta(\mathbf{k})/2$ can be seen as the vertex  supplied with such a weight factor. However, its coupling to other vertices gives only a contribution of order $\mathcal{O}(\varepsilon^3)$. Recall that we do not consider the constant part of Hamiltonian, which is independent of the field configuration and is represented by closed diagrams without external lines.

3.3 Estimation of \mathbf{k} -space integrals

It is important to know whether the \mathbf{k} -space integrals over the internal lines of the diagrams, appearing in our representation of the renormalized Hamiltonian, are convergent when the RG transformation is repeated unlimitedly many times, i. e., at $\zeta \rightarrow \infty$. We estimate such integrals in four dimensions to find the answer to this question.

First, we note that the diagram

$$\text{0} \cdot \text{---} \cdot \text{---} \cdot = \frac{1}{(2\pi)^4} \int_{\Lambda < q < \Lambda\zeta} \frac{d^4 q}{c^2 q^4} = \frac{K_4}{c^2} \int_{\Lambda}^{\Lambda\zeta} \frac{dq}{q} = \frac{K_4}{c^2} \ln \zeta \quad (33)$$

diverges when the region $q \in [\Lambda, \Lambda\zeta]$ of wave vectors for the internal lines is extended to $[\Lambda, \infty]$, i. e., at $\zeta \rightarrow \infty$. Similar diagram, where the zero- \mathbf{k} contribution is subtracted,

$$I(k) = \text{---} \cdot \text{---} \cdot = \text{---} \cdot \text{---} \cdot - \text{0} \cdot \text{---} \cdot , \quad (34)$$

is convergent. It can be shown by splitting the integration region $[\Lambda, \infty]$ in three parts as follows

$$I(k) = \frac{1}{(2\pi)^4 c^2} \left\{ \int_{\Lambda < q < k/C} f(q, k) d^4 q + \int_{k/C < q < kC} f(q, k) d^4 q + \int_{q > kC} f(q, k) d^4 q \right\} , \quad (35)$$

where

$$f(q, k) = q^{-2} |\mathbf{q} - \mathbf{k}|^{-2} \Theta(|\mathbf{q} - \mathbf{k}| - \Lambda) - q^{-4} , \quad (36)$$

$\Theta(x)$ is the step function (0 for $x < 0$ and 1 for $x > 0$), and C is a large constant. The first integral vanishes for $k < C\Lambda$ and is equal to $-(K_4/c^2) \ln k + \mathcal{O}(1)$ for $k > C\Lambda$, where $\mathcal{O}(1)$ is a quantity which is finite for any k . It is consistent with the approximation $|\mathbf{q} - \mathbf{k}| \approx k$ valid for $q \ll k$. The second integral is finite for all (positive) k . It can be verified by considering $\mathbf{q} - \mathbf{k}$ as a new integration variable, when evaluating the part of this integral without the q^{-4} term, and replacing q^{-2} with its maximal value $(k/C)^{-2}$ to estimate the upper bond.

Finally, the third integral in (35) can be evaluated changing from the decart coordinates q_x, q_y, q_z, q_w to the spherical ones: $q_x = q \cos \theta$, $q_y = q \sin \theta \cos \theta_1$, $q_z = q \sin \theta \sin \theta_1 \sin \varphi$, $q_w = q \sin \theta \sin \theta_1 \cos \varphi$, where $\theta \in [0, \pi]$, $\theta_1 \in [0, \pi]$, and $\varphi \in [0, 2\pi]$ are angles in this case. The integral $I(k)$ (where $dq_x dq_y dq_z dq_w \rightarrow q^3 \sin^2 \theta \sin \theta_1 dq d\theta d\theta_1 d\varphi$) then reads

$$I(k) = \frac{1}{4\pi^3 c^2} \int_{\Lambda}^{\infty} q dq \int_0^{\pi} \left\{ \frac{\Theta(q^2 - 2kq \cos \theta + k^2 - \Lambda^2)}{q^2 - 2kq \cos \theta + k^2} - \frac{1}{q^2} \right\} \sin^2 \theta d\theta . \quad (37)$$

The argument of the theta-function is positive for $k > C\Lambda$ and $q > Ck$ if C is large. For $k < C\Lambda$, the argument is always positive if $q > \tilde{q}_0$, where \tilde{q}_0 is some finite constant. Hence, the theta-function always can be replaced with 1 for q exceeding some finite value \tilde{q}_0 , when evaluating the integral over the range $q > Ck$. In this case the integrand can be expanded in powers of k/q and integrated term by term. It shows that the integral is convergent for any given k . Besides, the contribution of large wave vectors $q > q_0$ decreases as q_0^{-2} at $q_0 \rightarrow \infty$, and the integral over $q > Ck$ is finite for any k . Summarizing the analysis of (35), we conclude that

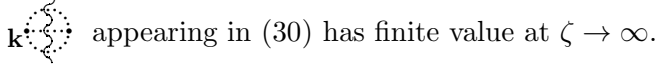
$$I(k) = -\frac{K_4}{c^2} \ln k + \mathcal{O}(1) \quad (38)$$

holds for $k > C\Lambda$, where the only divergent at $k \rightarrow \infty$ contribution comes from the first integral in (35).

Based on this result, we can evaluate the large- \mathbf{q} (i. e., $\Lambda C < q < \Lambda\zeta$ for large enough C at a given k) contribution to the diagram  as

$$\begin{aligned} & \frac{1}{(2\pi)^4 c} \int_{\Lambda C < q < \Lambda\zeta} [I(|\mathbf{k} + \mathbf{q}|) - I(q)] q^{-2} d^4 q \\ & \simeq -\frac{K_4}{8\pi^3 c^3} \int_{\Lambda C}^{\Lambda\zeta} q dq \int_0^\pi \ln \left(1 + \frac{2kq \cos \theta + k^2}{q^2} \right) \sin^2 \theta d\theta. \end{aligned} \quad (39)$$

Using the expansion in powers of k/q , we see that (39) logarithmically diverges at $\zeta \rightarrow \infty$. However, if we subtract the term $\propto k^2$, the result is convergent. It implies that the diagram



appearing in (30) has finite value at $\zeta \rightarrow \infty$.

Similarly, we can treat the large-wave-vector contribution to the diagram  further considered in the renormalization up to the order of ε^3 . This graph contains the subtraction of the zero-vector contribution from the internal block , as well as from the whole diagram. It is defined by

$$\mathbf{k} \otimes \mathbf{q} = \frac{1}{(2\pi)^4 c^2} \int_{\Lambda < q_1 < \Lambda\zeta} \left\{ q_1^{-2} |\mathbf{q}_1 + \mathbf{k}|^{-2} \hat{\Theta}(|\mathbf{q}_1 + \mathbf{k}|, \zeta) I(|\mathbf{q} - \mathbf{q}_1|) - q_1^{-4} I(q_1) \right\} d^4 q_1, \quad (40)$$

where $\hat{\Theta}(k, \zeta)$ is the cut function having the value 1 within $k \in [\Lambda, \Lambda\zeta]$ and zero otherwise. Using (38), we find that the tail of large q_1 is convergent for any given \mathbf{k} and \mathbf{q} .

The actual integrals have been estimated in four dimensions ($d = 4$). It is important to notice that those ones, which are convergent at $d = 4$, are convergent also in $d = 4 - \varepsilon$ dimensions for small (positive and also negative) ε , when considering the \mathbf{k} -space integrals as continuous functions of d in the usual sense of the ε -expansion. It is because the contribution of large wave vectors, $q > q_0$, changes only slightly.

3.4 Testing the semigroup property

Here we test the semigroup property

$$R_{s_1 s_2} \mu = R_{s_2} R_{s_1} \mu \quad (41)$$

discussed already in Sec. 1. In fact, we verify that the renormalized Hamiltonian after two subsequent RGT with scale factors s_1 and s_2 is the same as after one RGT with the scale factor $s_1 s_2$. It can be seen most easily for the vertices $\rightarrow \dots \leftarrow$ and $\rightarrow \dots \leftarrow$, as consistent with Eqs. (18) to (20) and the fact that u is renormalized only by an amount of $\mathcal{O}(\varepsilon^2)$. The semigroup property for the coupling constant u easily follows from (21). After the first RGT we have

$$u' = s_1^\varepsilon \left[u - \frac{n+8}{2} u^2 \mathbf{0} \otimes \mathbf{0} \right] + \mathcal{O}(\varepsilon^3), \quad (42)$$

where the dotted line refers to the k interval $[\Lambda/s_1, \Lambda]$. After the second RGT the value of the coupling constant, denoted as u'' , becomes

$$u'' = s_2^\varepsilon \left[u' - \frac{n+8}{2} u'^2 s_1^{-\varepsilon} \text{ (dotted line)} \right] + \mathcal{O}(\varepsilon^3), \quad (43)$$

where the dashed line refers to the interval $[\Lambda/(s_1 s_2), \Lambda/s_1]$. Here the rescaling of the wave vectors from $k \in [\Lambda/s_2, \Lambda]$ to $k \in [\Lambda/(s_1 s_2), \Lambda/s_1]$ has been performed for convenience. Inserting (42) in (43), and taking into account that $u = \mathcal{O}(\varepsilon)$, we obtain

$$\begin{aligned} u'' &= (s_1 s_2)^\varepsilon \left[u - \frac{n+8}{2} u^2 \left\{ \text{ (dotted line)} + \text{ (dashed line)} \right\} \right] + \mathcal{O}(\varepsilon^3) \\ &= (s_1 s_2)^\varepsilon \left[u - \frac{n+8}{2} u^2 \text{ (dashed line)} \right] + \mathcal{O}(\varepsilon^3), \end{aligned} \quad (44)$$

where $k \in [\Lambda/(s_1 s_2), \Lambda]$ corresponds to the solid coupling lines. It is obvious that (44) is identical to the result of one RGT obtained from (21) with $s = s_1 s_2$, which proves the semigroup property. Analogous diagram summation proves this property also in the next order of the ε -expansion [13].

The semigroup property for the parameter r , when performing the RG transformations of the initial Hamiltonian with $\zeta = 1$, is proven straightforwardly by the same method. Namely, the result of the second RGT (applying (22)) is represented by the diagrams containing the dotted and the dashed lines with $k \in [\Lambda/s_1, \Lambda]$ and $k \in [\Lambda/(s_1 s_2), \Lambda/s_1]$, respectively. These diagrams sum up to give ones with $k \in [\Lambda/(s_1 s_2), \Lambda]$, which correspond to those of the one-step renormalization with $s = s_1 s_2$. In distinction to the case of u , here more complicated terms appear, including different lines in one diagram. The situation is less trivial when starting with $\zeta > 1$. In this case all diagrams can be decomposed in such ones, which contain three types of lines with $k \in [\Lambda, \Lambda\zeta]$, $k \in [\Lambda/s_1, \Lambda]$ and $k \in [\Lambda/(s_1 s_2), \Lambda/s_1]$, respectively. Then we prove the semigroup property by checking that such diagram representation for the two-step renormalization is identical (up to the considered order of the ε -expansion) to that for the one-step renormalization. The semigroup property for the parameters c and $\theta(\mathbf{k})$ is proven by this method, as well.

3.5 The fixed point

The RG flow described by the truncated perturbative equations of Sec. 3.1 has certain fixed point as a steady state solution of the RG flow equations. We shall mark the fixed-point values by an asterisk, except the value of c , since the fixed point exists for any given c , as it will be seen from the following analysis. The fixed-point value of the coupling constant u , i. e.,

$$u^* = \frac{2c^2}{(n+8)K_4} \varepsilon + \mathcal{O}(\varepsilon^2) \quad (45)$$

has been already mentioned in Sec. 3.1. According to (19) and (20), we have $a_4^* = -(9u^{*2})/16 + \mathcal{O}(\varepsilon^3)$ and $a_6^* = -u^{*2}/8 + \mathcal{O}(\varepsilon^3)$. It is generally expected that the fixed point is independent of the scale parameter s . In the exact renormalization, it is a consequence of the semigroup property. In the perturbation theory, it is expected to hold at each order of the expansion. The above considered fixed-point values obey this requirement within the given accuracy. It is obviously true also for the r^* value in the lowest order of the expansion, i. e.,

$$r^* = -\frac{c\Lambda^2}{2} \frac{n+2}{n+8} \varepsilon + \mathcal{O}(\varepsilon^2). \quad (46)$$

However, it is less obvious for the next-order correction to r^* , as well as for other parameters of the fixed-point Hamiltonian. Therefore, we have performed some tests. Using (45), (19), and (20), we find from (22) that r^* is independent of s within the error of $\mathcal{O}(\varepsilon^3)$ if

$$f(s) = -\frac{3}{2} \frac{K_4^2 \Lambda^2}{c^3} \ln s + \text{const} \cdot (s^2 - 1) \quad (47)$$

holds, where

$$f(s) = s^2 \left\{ \text{0} \bigcirclearrowleft + 3 \sum_{i=1}^2 \lim_{\zeta \rightarrow \infty} D_i(\Lambda/s, \Lambda, \Lambda\zeta) \right\}. \quad (48)$$

Here the solid lines have wave vectors within $k \in [\Lambda/s, \Lambda]$ and all terms are evaluated at $d = 4$. On the other hand, we prove that the function (48) obeys the equation

$$s_2^2 f(s_1) + f(s_2) = f(s_1 s_2) - 3 \text{0} \bigcirclearrowleft \times \text{0} \cdots \bigcirclearrowleft \times (s_1 s_2)^2, \quad (49)$$

where the dashed lines refer to the interval $k \in [\Lambda/(s_1 s_2), \Lambda/s_1]$ and the dotted lines — to the interval $k \in [\Lambda/s_1, \Lambda]$. The proof consists of a straightforward checking of the corresponding diagram identity by the decomposition described at the end of Sec. 3.4. Note only that the wave vectors in the diagrams of $f(s_2)$ are rescaled by the factor $1/s_1$. As a test of consistency, we verify that (47) is a solution of (49).

As regards the parameter c , it appears as a common factor in the fixed-point equation obtained by setting $c' = c$ and $u = u^*$ in (25), taking into account that $u^* \propto c^2$, whereas the diagrams involved are proportional to $1/c^3$. Hence, if this equation is satisfied, then it holds for any c . In fact, the equation $c' = c$ reduces to one for the exponent η :

$$\eta \ln s = -\frac{2(n+2)}{(n+8)^2 K_4^2} \tilde{\Pi}(s) \varepsilon^2 + \mathcal{O}(\varepsilon^3), \quad (50)$$

where

$$\tilde{\Pi}(s) = \lim_{\zeta \rightarrow \infty} \lim_{k \rightarrow 0} \left\{ k^{-2} \left[\text{k} \bigcirclearrowleft - \text{0} \bigcirclearrowleft + 3 \left(\text{k} \cdots \bigcirclearrowleft - \text{0} \cdots \bigcirclearrowleft + \text{k} \bigcirclearrowleft \cdots - \text{0} \cdots \bigcirclearrowleft \right) \right] \Big|_{c=1} \right\} \quad (51)$$

is calculated at $d = 4$ with $k \in [\Lambda/s, \Lambda]$ corresponding to the solid lines and $k \in [\Lambda, \Lambda\zeta]$ — to the dotted lines in the diagrams. The expected universality of the critical exponent η follows from the diagram identity

$$\tilde{\Pi}(s_1) + \tilde{\Pi}(s_2) = \tilde{\Pi}(s_1 s_2), \quad (52)$$

which implies that $\tilde{\Pi}(s) \propto \ln s$ holds and, therefore, η is independent of s . The identity (52) is proven by the same method as (49). In principle, the critical exponent η can be calculated from (50) at any given s . However, from a technical point of view, it is convenient to consider the limit $s \rightarrow \infty$, since only the first two diagrams in (51) provide the singular contribution $\sim \ln s$ in this case. Hence, we have

$$\eta = -\frac{2(n+2)}{(n+8)^2 K_4^2} \varepsilon^2 \times \lim_{s \rightarrow \infty} \lim_{k \rightarrow 0} \left\{ \frac{1}{k^2 \ln s} \left(\text{k} \bigcirclearrowleft - \text{0} \bigcirclearrowleft \right) \Big|_{c=1} \right\} + \mathcal{O}(\varepsilon^3). \quad (53)$$

Evaluation of the \mathbf{k} -space integrals in four dimensions by the standard methods [2] yields the well known result

$$\eta = \frac{1}{2} \frac{n+2}{(n+8)^2} \varepsilon^2 + \mathcal{O}(\varepsilon^3). \quad (54)$$

Closing this section, we note that the independence of the fixed-point function $\theta^*(\mathbf{k})$ on the RGT scale parameter s can be easily seen when using the diagrammatic representation (30), taking into account that this diagram converges to certain s -independent value at $\zeta \rightarrow \infty$, as shown in Sec. 3.3.

4 A refined diagrammatic renormalization

Here we consider a refined renormalization scheme, taking into account the correction terms omitted in the derivations of Sec. 3.2. In this case the only approximation is that the vertices of higher than $\mathcal{O}(\varepsilon^2)$ orders are omitted.

To simplify the notation, consider first the one-component case $n = 1$, where the symbol Σ in (17) can be omitted. The dashed lines, similarly as dotted and solid coupling lines, are related to the propagator $1/(ck^2)$ in the notations used in this section.

After m RG transformations with a constant scale factor s , the terms with a_4 and a_6 in (17) now look as

$$\sum_{j,l=1}^m (a_4)_{jl} \left(\begin{array}{c} > \cdots \times \cdots \leftarrow \\ \hline \end{array} \right)_{jl}, \quad (55)$$

$$\sum_{j=1}^m (a_6)_j \left(\begin{array}{c} \Rightarrow \cdots \leftarrow \\ \hline \end{array} \right)_j, \quad (56)$$

where the indices j and l are used to distinguish between diagrams with different k intervals related to the coupling lines. Namely, the dotted lines in the diagrams refer to $k \in [\Lambda s^{j-1}, \Lambda s^j]$, whereas the dashed line — to $k \in [\Lambda s^{l-1}, \Lambda s^l]$. In the RG flow equations of Sec. 3.1 we have $(a_4)_{jl} = a_4$ and $(a_6)_j = a_6$, whereas here these weight coefficients are slightly different.

The generalisation to the n -component case is possible by using the decompositions of the kind (55) and (56) for the diagram of each topology when deciphered as one composed of the vertices  instead of .

Within the $\mathcal{O}(\varepsilon^3)$ error of the actual truncation scheme, the weight coefficients $(a_4)_{jl}$ and $(a_6)_j$ after m RG transformations, i. e., $(a_4)_{jl}(m)$ and $(a_6)_j(m)$, are given by the recurrence relations

$$(a_6)_1(m) = -\frac{1}{8}R_m s^{2\varepsilon-3\eta} u^2(m-1) \quad (57)$$

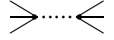
$$(a_6)_j(m) = R_m s^{2\varepsilon-3\eta} (a_6)_{j-1}(m-1) \quad : \quad 2 \leq j \leq m, m \geq 2 \quad (58)$$

$$(a_4)_{11}(m) = -\frac{9}{16}R_m^2 s^{2\varepsilon-2\eta} u^2(m-1) \quad (59)$$

$$(a_4)_{1j}(m) = (a_4)_{j1}(m) = \frac{9}{2}R_m^2 s^{2\varepsilon-2\eta} (a_6)_{j-1}(m-1) \quad : \quad 2 \leq j \leq m, m \geq 2 \quad (60)$$

$$(a_4)_{jl}(m) = R_m^2 s^{2\varepsilon-2\eta} (a_4)_{j-1,l-1}(m-1) \quad : \quad 2 \leq j \leq m, 2 \leq l \leq m, m \geq 2 \quad (61)$$

where $R_m = c(m)/c(m-1)$ is the ratio of c values in two subsequent RG transformations. We have denoted by $u(m)$ and $c(m)$ the values of u and c , respectively, after the m -th RGT, the initial values being given by $u(0)$ and $c(0)$. Eq. (57) represents the contribution due to the coupling like  and rescaling of two ordinary φ^4 vertices, whereas the coefficients (58) are the weight factors of the corresponding terms rescaled repeatedly. Eq. (59) corresponds to the coupling and rescaling of two ordinary φ^4 vertices like  , whereas (60) — to the

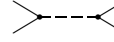
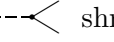
coupling of two lines of the vertex  with $k \in [\Lambda s^{j-2}, \Lambda s^{j-1}]$ related to the dotted line, followed by the rescaling of the diagram. Although there are 9 combinatorial possibilities to couple these lines, the factor $9/2$ in (60) is twice smaller. It is because the corresponding term appears twice in the decomposition (55), i. e., as $(a_4)_{1j}$ and $(a_4)_{j1}$. Finally, (61) comes from the rescaling of the quartic terms (59) and (60). The actual update rules (57) to (61) are consistent with the fact that the range of the wave vectors for the internal lines of any diagram is rescaled by the factor s in each RGT, taking into account the corresponding rescaling factors discussed in previous sections. Here, however, additional rescaling factors R_m and R_m^2 appear, which have been neglected before. They originate from the renormalization of parameter c : since the diagrams are defined so that factors $1/(ck^2)$ correspond to the coupling lines, these factors need to be redefined with new value of c after each RGT. Hence, the weight coefficient for a diagram with l such coupling lines gets a factor R_m^l .

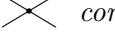
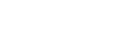
Eqs. (57) to (61) can be applied also to the general n -component case. In this case $(a_4)_{jl}$ are the common factors for the weighted sum of diagrams of three different topologies appearing in (14) with the corresponding k intervals for the coupling lines. It is obviously true because the diagrams of these three topologies always appear with certain relative weight factors, which depend only on n and are the same as in (14).

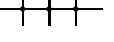
Since u and c are varied only by an amount of $\mathcal{O}(\varepsilon^2)$ in one RGT, it is easy to verify that Eqs. (57) to (61) provide $(a_4)_{jl}(m) = (a_4)_{11}(m) + \mathcal{O}(\varepsilon^3)$ and $(a_6)_j(m) = (a_6)_1(m) + \mathcal{O}(\varepsilon^3)$ for any m and $j \leq M$, $l \leq M$ at any large but finite M . Besides the values of these coefficients are consistent within the $\mathcal{O}(\varepsilon^3)$ error with the corresponding values of a_4 and a_6 provided by (19) and (20) after m RG transformations. Since the diagram  is convergent when the wave vectors within $[\Lambda, \infty]$ are related to the dotted lines (see Sec. 3.3), the contribution of infinitely large wave vectors is unimportant here. Hence, calculations here and in Sec. 3 yield consistent estimates of the renormalized Hamiltonian.

5 Renormalization up to the order of ε^3

5.1 Vertices of the order $\mathcal{O}(\varepsilon^3)$

According to our diagrammatic representation, vertices of the order $\mathcal{O}(\varepsilon^3)$ in the renormalized Hamiltonian are those made by coupling three original vertices of (2), as well as other diagrams of such topology. The following rigorous statements are used to find the topological pictures, made by coupling lines, corresponding to the vertices of the order $\mathcal{O}(\varepsilon^3)$. These are the topological pictures obtained when the dashed lines of the vertices  shrink to points, so that we deal with  instead.

Lemma 1. *Any connected diagram made of three vertices  contains a subset of two coupling lines connecting the nodes as in the diagram .*

Proof. Let number the vertices as vertex 1, vertex 2, and vertex 3. Since the diagram is connected, vertex 1 has to be connected at least with one line either to vertex 2 or to vertex 3. In the first case vertex 3 has to be connected at least with one line either to vertex 1 or to vertex 2 to make a connected diagram. Similarly, in the second case vertex 2 has to be connected at least with one line either to vertex 1 or to vertex 3. Hence such a subset of connecting lines as in the diagram  always exists. \square

Lemma 2. *Any diagram of the renormalized Hamiltonian containing a subgraph (which is not the whole diagram) of topology  ,  ,  ,  ,  , etc., i. e., a subgraph with two outgoing lines, can be nonvanishing only if the lines of this subgraph are the internal ones of the whole diagram.*

Proof. The considered subgraphs have opposite wave vectors \mathbf{k} and $-\mathbf{k}$ related to their two outgoing lines, as it follows from the fact that the sum of the wave vectors entering each node in a Feynman diagram is vanishing. On the other hand, by definition of the RGT, the internal and the external lines in the diagrams of the renormalized Hamiltonian always have different values of $|\mathbf{k}|$. Hence, the diagram can be nonvanishing only if both outgoing lines of the subgraph are either internal or external lines of the whole diagram. Only the first scenario is possible, since the subgraph has to be connected to the rest of the diagram. \square

Lemma 3. *Any connected diagram with at least four external lines, which is a nonvanishing diagram of the renormalized Hamiltonian and is made of two vertices  and one vertex  , contains a subset of two coupling lines connecting the nodes as in the graph  .*

Proof. The lines of the vertex  have to be the internal lines of the diagram according to *Lemma 2*. Hence, there are two possible ways how these lines can be coupled to the rest of the diagram: (1) they are connected to two lines of one of the vertices  as  ; and (2) they are connected to both vertices  as  . In the first case, the remaining vertex  has to be connected as  to obtain a diagram with at least four external lines. This diagram, however, is vanishing according to *Lemma 2*. Hence, only the second possibility remains, i. e., the subset of coupling lines contained in the diagram  always exists. \square

It is easy to verify that nonvanishing connected diagrams made of two vertices  and one vertex  can contain no more than two external lines. Thus, *Lemma 1* and *Lemma 3* imply that the diagrams of order $\mathcal{O}(\varepsilon^3)$ with at least four external lines can have only the following topologies:  ,  , and those ones obtained by coupling the lines in these graphs. Using also *Lemma 2*, it allows to find easily all the nonvanishing diagrams of this type. In such a way, the renormalized Hamiltonian has the form

$$H = H^{(2)} + H^{(4)} + H^{(6)} + H^{(8)} + \mathcal{O}(\varepsilon^4), \quad (62)$$

where $H^{(2m)}$ includes all the φ^{2m} -type vertices representable by the diagrams with $2m$ external lines. The corresponding algebraic representation is

$$\frac{H^{(2m)}}{T} = V^{1-m} \sum_{i_1, \dots, i_m} \sum_{\mathbf{k}_1, \mathbf{q}_1, \dots, \mathbf{k}_m, \mathbf{q}_m} Q_m(\mathbf{k}_1, \mathbf{q}_1, \dots, \mathbf{k}_m, \mathbf{q}_m) \varphi_{i_1, \mathbf{k}_1} \varphi_{i_1, \mathbf{q}_1} \cdots \varphi_{i_m, \mathbf{k}_m} \varphi_{i_m, \mathbf{q}_m}. \quad (63)$$

In such a form $Q_m(\mathbf{k}_1, \mathbf{q}_1, \dots, \mathbf{k}_m, \mathbf{q}_m)$ vanishes unless $\sum_i \mathbf{k}_i + \mathbf{q}_i = \mathbf{0}$. The dependence of these weight factors on various parameters is not indicated here.

In the following we will treat only the terms with $m \geq 2$, including the diagrams of the above considered topologies. As regards the quartic part $H^{(4)}$, we separate the contribution corresponding to the ordinary φ^4 vertex, which is provided by the constant part of the weight function $\bar{Q}(\mathbf{0}, \mathbf{0}, \mathbf{0}, s, n, \varepsilon)$ in (8), i. e., of the constant part of Q_2 in (63). For this purpose we

represent each diagram of $H^{(4)}$ as

$$\text{Diagram} = \text{Diagram} + \text{Diagram} \times \text{Diagram} . \quad (64)$$

In this symbolic notation  is any diagram with four external lines, whereas  is the same diagram from which the contribution corresponding to the ordinary φ^4 vertex is subtracted. The latter one is represented by the last term in (64), where  is the diagram with amputated external lines having zero wave vectors. A particular example

$$\text{Diagram} = \text{Diagram} + \text{Diagram} \times \text{Diagram} \quad (65)$$

refers to the diagrams already considered in Sec. 3.

5.2 An approximate form of the renormalized Hamiltonian

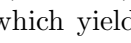
For or a finite number (m) of RG transformations, it is possible to represent the renormalized Hamiltonian up to the order of ε^3 in the form, where the wave vectors within $k \in [\Lambda, \Lambda\zeta]$ (with the parameter ζ updated as $\zeta' = s\zeta$) are related to all internal lines of the diagrams. The proof of this statement consists of a direct verification, as in Sec. 3. In distinction to the previous case (Sec. 3), such a form is not always valid at $m \rightarrow \infty$ in the calculations up to the order of ε^3 , as discussed in Sec. 5.3. Nevertheless, it is convenient to show the structure of the renormalized Hamiltonian.

Based on the diagram analysis in Sec. 5.1 and the actual considerations, the parts of the renormalized Hamiltonian after a finite number of RGT can be represented as

$$\begin{aligned} \frac{H^{(4)}}{T} &= \frac{u}{8} \text{Diagram} + a_4^{(1)} \Sigma \left(\text{Diagram} \right) + a_4^{(2)} \Sigma \left(\text{Diagram} \right) \\ &+ a_4^{(3)} \Sigma \left(\text{Diagram} \right) + a_4^{(4)} \Sigma \left(\text{Diagram} \right) + \mathcal{O}(\varepsilon^4) \end{aligned} \quad (66)$$

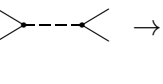
$$\begin{aligned} \frac{H^{(6)}}{T} &= a_6^{(1)} \Sigma \left(\text{Diagram} \right) + a_6^{(2)} \Sigma \left(\text{Diagram} \right) \\ &+ a_6^{(3)} \Sigma \left(\text{Diagram} \right) + a_6^{(4)} \Sigma \left(\text{Diagram} \right) + \mathcal{O}(\varepsilon^4) \end{aligned} \quad (67)$$

$$\frac{H^{(8)}}{T} = a_8 \Sigma \left(\text{Diagram} \right) + \mathcal{O}(\varepsilon^4) , \quad (68)$$

where, similarly as before, $\Sigma(\cdot)$ denotes the sum of all such diagrams made of vertices  and  (depicting the coupling lines as dotted ones related to $k \in [\Lambda, \Lambda\zeta]$), which yield the given picture when the dashed lines shrink to points. Besides, the combinatorial weight coefficients, including the n -dependent factors, are normalized in such a way that their sum is 1 at $n = 1$. This notation is completely analogous to (14). Here the relations

$$\text{Diagram} = \text{Diagram} \times \text{Diagram} \quad (69)$$

$$\text{Diagram} = \text{Diagram} \times \text{Diagram} \quad (70)$$

have been applied to reduce the number of different kind of vertices in the representation of the Hamiltonian. As usually, by such a notation we mean diagrams obtained when  \rightarrow .

5.3 RG flow equations up to the order of ε^3

Let us consider now the problem of convergence of the RG flow to some fixed-point Hamiltonian, starting with (1) where $u = \mathcal{O}(\varepsilon) > 0$, $r = \mathcal{O}(\varepsilon)$, and c is a positive constant of order unity. It is seen already from the RG flow equation for u up to the order of ε^2 (10) that this coupling constant changes asymptotically slowly in the renormalization procedure at $\varepsilon \rightarrow 0$. Namely, it is varied only by an amount of $\sim \varepsilon^2 \ln s$ in one RGT with a finite scale parameter s . Besides, one needs to perform $m \gg 1/(\varepsilon \ln s)$ such RG transformations to obtain a value which is much closer to the fixed point as compared to the initial value. It means that the RG flow equations, which are valid only for finite m , are not appropriate to study the convergence (or non-convergence) of the RG flow to the fixed point.

In the following we will consider certain truncation scheme, using the representation (64) for quartic terms and one without the subtraction of zero- \mathbf{k} contributions for vertices with more than 4 external lines. Namely, we will omit the diagrams of higher than $\mathcal{O}(\varepsilon^3)$ orders in such a representation. The approximate form (66) — (68) is not valid here, since a precise calculation shows essential deviations from it at $m \rightarrow \infty$. We will use a refined scheme similar to that outlined in Sec. 4, with the only difference that now the calculations are performed including the terms of order $\mathcal{O}(\varepsilon^3)$. Such a decomposition of vertices is more general and the form is absolutely stable in the sense that the renormalized Hamiltonian always can be represented in this way when considering the sequence of RG transformations with given scale factor s .

In this method, the structure of the renormalized Hamiltonian can be deduced from that considered in Sec. 5.2: the wave-vector-interval $[\Lambda, \Lambda\zeta]$ for each of the internal lines now is split in subintervals, decomposing each diagram like in (55) and (56). To simplify the notation, we will consider first the one-component case $n = 1$, as in Sec. 4. The diagrams with $a_4^{(1)}$, $a_4^{(2)}$, and $a_4^{(3)}$ in (66) now are replaced by the corresponding decompositions:

$$\sum_{j,l=1}^m (a_4^{(1)})_{jl} \left(\begin{array}{c} \diagup \dots \diagdown \\ \diagdown \dots \diagup \end{array} \right)_{jl}, \quad (71)$$

$$\sum_{i_1, i_2, j_1, j_2=1}^m (a_4^{(2)})_{i_1 i_2 j_1 j_2} \left(\begin{array}{c} \diagup \dots \diagdown \\ \diagdown \dots \diagup \\ \diagup \dots \diagdown \end{array} \right)_{i_1 i_2 j_1 j_2}, \quad (72)$$

$$\sum_{i_1, i_2, j_1, j_2=1}^m (a_4^{(3)})_{i_1 i_2 j_1 j_2} \left(\begin{array}{c} \diagup \dots \diagdown \\ \diagdown \dots \diagup \\ \diagup \dots \diagdown \\ \diagup \dots \diagdown \end{array} \right)_{i_1 i_2 j_1 j_2}, \quad (73)$$

where the indices label wave-vector-intervals (i -th interval is $[\Lambda s^{i-1}, \Lambda s^i]$) for different internal lines in the diagrams, like in Sec. 4. Besides, the indices i_1 and i_2 in (72) and (73) refer to the two coupling lines on the left hand side in the corresponding diagrams. Here the couplings are shown by different lines, since in general they correspond to different intervals of the wave vectors. All other diagrams are decomposed similarly.

The RG flow equations are the update rules for the decomposition weight coefficients. It is difficult to analyse all of them. However, a subset of quartic terms can be calculated independently of all other contributions. Namely, omitting the diagrams of higher than $\mathcal{O}(\varepsilon^3)$ orders,

the values of $(a_4^{(1)})_{jj}$, $(a_4^{(2)})_{11jj}$, and $(a_4^{(3)})_{11jj}$ after the m -th RGT with a given scale factor s , i. e., $(a_4^{(1)})_{jj}(m)$, $(a_4^{(2)})_{11jj}(m)$, and $(a_4^{(3)})_{11jj}(m)$, are calculated out of a relatively simple recurrence relations

$$(a_4^{(1)})_{11}(1) = -\frac{9}{16}R_1^2 s^{2\varepsilon-2\eta} u^2(0) \quad (74)$$

$$(a_4^{(1)})_{11}(m) = -R_m^2 s^{2\varepsilon-2\eta} \left[\frac{9}{16}u^2(m-1) - 9u(m-1) \sum_{j=1}^{m-1} (a_4^{(1)})_{jj}(m-1) b_j(m-1) \right] : m \geq 2 \quad (75)$$

$$(a_4^{(1)})_{jj}(m) = R_m^2 s^{2\varepsilon-2\eta} (a_4^{(1)})_{j-1,j-1}(m-1) : 2 \leq j \leq m, m \geq 2 \quad (76)$$

$$(a_4^{(2)})_{1111}(m) = \frac{27}{32}R_m^4 s^{3\varepsilon-2\eta} u^3(m-1) \quad (77)$$

$$(a_4^{(3)})_{1111}(m) = \frac{27}{8}R_m^4 s^{3\varepsilon-2\eta} u^3(m-1) \quad (78)$$

$$\begin{aligned} (a_4^{(2)})_{11jj}(m) &= (a_4^{(2)})_{jj11}(m) \\ &= -\frac{3}{2}R_m^4 s^{3\varepsilon-2\eta} u(m-1) (a_4^{(1)})_{j-1,j-1}(m-1) : 2 \leq j \leq m, m \geq 2 \end{aligned} \quad (79)$$

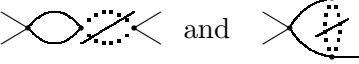
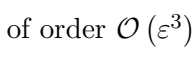
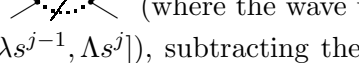
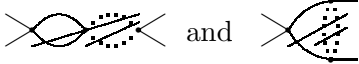
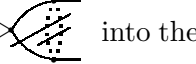
$$(a_4^{(3)})_{11jj}(m) = -6R_m^4 s^{3\varepsilon-2\eta} u(m-1) (a_4^{(1)})_{j-1,j-1}(m-1) : 2 \leq j \leq m, m \geq 2 \quad (80)$$

where $b_j(m)$ is the value of the diagram  with $k \in [\Lambda s^{j-1}, \Lambda s^j]$ corresponding to the coupling lines. In $4 - \varepsilon$ dimensions it is

$$b_j(m) = \frac{K_d}{\Lambda^\varepsilon c^2(m)} \frac{s^\varepsilon - 1}{\varepsilon} s^{-j\varepsilon}. \quad (81)$$

Other notations (R_m , $u(m)$, $c(m)$) are already introduced in Sec. 4.

Eqs. (74) to (76) for $(a_4^{(1)})_{jj}(m)$ are consistent with (and have the same origin as) the corresponding equations (59) and (61) for $(a_4)_{jj}$ in a lower order of the diagram expansion, with the only difference that now Eq. (75) contains a correction term. It comes from the diagrams

 and  of order $\mathcal{O}(\varepsilon^3)$ obtained by coupling the ordinary φ^4 vertex to  (where the wave vectors of the dotted lines can belong to any of the intervals $[\Lambda s^{j-1}, \Lambda s^j]$), subtracting the part corresponding to the ordinary φ^4 vertex, and transforming the obtained graphs  and  into the form (64) according to the identities

$$\begin{aligned} \text{Diagram 1} &= \text{Diagram 2} - 0 \cdot \text{Diagram 3} \times \text{Diagram 4} \end{aligned} \quad (82)$$

$$\begin{aligned} \text{Diagram 5} &= \text{Diagram 6} - 0 \cdot \text{Diagram 7} \times \text{Diagram 8} . \end{aligned} \quad (83)$$

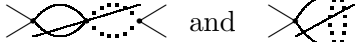
In this case, the second vertex on the right hand side of (82) and (83) yields the considered correction term in (75) after the rescaling step of RGT. This term contains factors $u(m-1)$

and $(a_4^{(1)})_{jj}(m-1)$, as it originates from vertices  and . It includes also the coefficient $b_j(m-1)$ coming from .

The terms on the right hand side of (77) and (78) represent the only relevant at this order of the perturbation theory contributions, related to the case where $k \in [\Lambda, \Lambda s]$ holds for all

coupling lines in the diagrams  and . These come (after the rescaling step) from the coupling of three ordinary φ^4 vertices to form the actual diagrams.

Finally, Eqs. (79) and (80) are consistent with the fact that the only relevant here contributions, which are related to the indicated (by the indices $11jj$) intervals of the wave vectors in

the diagrams  and  come from the already considered in Eqs. (82) and (83) diagrams. In this case the (rescaled) first vertex on the right hand side of (82) and the corresponding one in (83) are involved, yielding the contributions to (79) and (80), respectively.

It is easy to verify that all terms in (74) to (80) are already included, if the perturbation expansion is truncated omitting the diagrams of higher than $\mathcal{O}(\varepsilon^3)$ orders.

5.4 Instability of the RG flow

In this section we present our most interesting result. Namely, we prove that, in the case if the coupling constant u as well as the parameter c behave in an expected and reasonable way, the quartic terms are rapidly divergent at $m \rightarrow \infty$.

Theorem. *If there exist positive constants u_{min} and c_{max} such that $u(m) > u_{min}$ and $0 < c(m) < c_{max}$ hold for all considered m , where $u(m)$ and $c(m)$ are the values of parameters u and c after m RG transformations with given scale factor s , then the weight coefficients in (71) obey the inequality $-(a_4^{(1)})_{11}(m) > a_{min}(m)$ for $m \geq 2$, where $a_{min}(m)$ is the lower bound*

$$a_{min}(m) = s^{2\varepsilon-2\eta} \left(\frac{c(m)}{c(m-1)} \right)^2 \left[\frac{9}{16} u^2(m-1) + 9 u(m-1) \mathcal{Q}(m) \right] \quad (84)$$

with

$$\mathcal{Q}(m) = \frac{9}{16} u_{min}^2 \left(\frac{c(m)}{c_{max}} \right)^2 \frac{K_d}{\Lambda^\varepsilon c^2(m-1)} \times \frac{s^\varepsilon - 1}{\varepsilon} \times \frac{s^{m(\varepsilon-2\eta)} - s^{\varepsilon-2\eta}}{s^{\varepsilon-2\eta} - 1}. \quad (85)$$

Proof. First we prove the inequality

$$-(a_4^{(1)})_{jj}(m) > \frac{9}{16} u_{min}^2 \left(\frac{c(m)}{c(m-j)} \right)^2 s^{2j(\varepsilon-\eta)} \quad : \quad 1 \leq j \leq m. \quad (86)$$

From (74) we find that (86) holds for $j = m = 1$. In the following we verify that (86) holds for $m = \ell$ and $j = 1, 2, \dots, \ell$ if this inequality is satisfied for $m = \ell - 1$. Namely, from (75) we find that (86) holds for $m = \ell$ and $j = 1$, since all terms of the sum are negative, as it follows from the fact that (86) is true for $m = \ell - 1$. According to the latter, (76) yields

$$\begin{aligned} -(a_4^{(1)})_{jj}(\ell) &> s^{2(\varepsilon-\eta)} \left(\frac{c(\ell)}{c(\ell-1)} \right)^2 \times \frac{9}{16} u_{min}^2 \left(\frac{c(\ell-1)}{c(\ell-1-[j-1])} \right)^2 s^{2(j-1)(\varepsilon-\eta)} \\ &= \frac{9}{16} u_{min}^2 \left(\frac{c(\ell)}{c(\ell-j)} \right)^2 s^{2j(\varepsilon-\eta)} \end{aligned} \quad (87)$$

for $2 \leq j \leq \ell$. It proves (86) by induction. Since $c(m) < c_{max}$ holds for all m , the inequality (86) can be replaced with

$$-\left(a_4^{(1)}\right)_{jj}(m) > \frac{9}{16}u_{min}^2 \left(\frac{c(m)}{c_{max}}\right)^2 s^{2j(\varepsilon-\eta)} \quad : \quad 1 \leq j \leq m. \quad (88)$$

Using (88) and (81), we estimate the sum in (75) as

$$-\sum_{j=1}^{m-1} \left(a_4^{(1)}\right)_{jj}(m-1) b_j(m-1) > \mathcal{Q}(m), \quad (89)$$

where $\mathcal{Q}(m)$ is given by (85). Inserting this into (75), we arrive to (84). \square

The above *Theorem* leads immediately to the lower bonds for the coefficients in (79) and (80) with $j = 2$:

$$\left(a_4^{(l)}\right)_{1122}(m) > C_l s^{3\varepsilon-2\eta} \left(\frac{c(m)}{c(m-1)}\right)^4 u(m-1) a_{min}(m-1), \quad (90)$$

where $l = 2, 3$ and C_l are constans, i. e., $C_2 = 3/2$ and $C_3 = 6$.

It is seen from (84), (85), and (90) that the parameters $\left(a_4^{(1)}\right)_{11}(m)$, as well as $\left(a_4^{(l)}\right)_{1122}(m)$ diverge at $m \rightarrow \infty$ for any small positive ε at $\eta = \mathcal{O}(\varepsilon^2)$, found in the ε -expansion, if u and c approach some finite and positive fixed-point values.

However, a cancellation of divergent terms takes place partly. It is seen when representing the quartic terms (71) to (73) after the final RGT as

$$\sum_{j,l=1}^m (A_4)_{jl} \left(\begin{array}{c} \diagup \dots \diagdown \\ \diagdown \dots \diagup \end{array} \right)_{jl}, \quad (91)$$

$$\sum_{i_1, i_2, j_1, j_2=1}^m \left(a_4^{(2)}\right)_{i_1 i_2 j_1 j_2} \left(\begin{array}{c} \diagup \dots \diagdown \\ \diagdown \dots \diagup \\ \text{---} \end{array} \right)_{i_1 i_2 j_1 j_2}, \quad (92)$$

$$\sum_{i_1, i_2, j_1, j_2=1}^m \left(a_4^{(3)}\right)_{i_1 i_2 j_1 j_2} \left(\begin{array}{c} \diagup \dots \diagdown \\ \diagdown \dots \diagup \\ \text{---} \\ \text{---} \end{array} \right)_{i_1 i_2 j_1 j_2}, \quad (93)$$

in accordance with the transformations

$$\begin{array}{c} \diagup \dots \diagdown \\ \diagdown \dots \diagup \end{array} = \begin{array}{c} \diagup \dots \diagdown \\ \diagdown \dots \diagup \\ \text{---} \end{array} + \text{0} \begin{array}{c} \dots \\ \diagup \dots \diagdown \end{array} \times \begin{array}{c} \diagup \dots \diagdown \\ \diagdown \dots \diagup \end{array} + \text{0} \begin{array}{c} \dots \\ \diagdown \dots \diagup \end{array} \times \begin{array}{c} \diagup \dots \diagdown \\ \diagdown \dots \diagup \end{array} \quad (94)$$

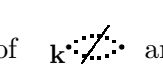
$$\begin{array}{c} \diagup \dots \diagdown \\ \diagdown \dots \diagup \\ \text{---} \end{array} = \begin{array}{c} \diagup \dots \diagdown \\ \diagdown \dots \diagup \\ \text{---} \end{array} + \text{0} \begin{array}{c} \dots \\ \diagup \dots \diagdown \end{array} \times \begin{array}{c} \diagup \dots \diagdown \\ \diagdown \dots \diagup \end{array}, \quad (95)$$

where the subtractions of zero- \mathbf{k} contributions from each of the diagram blocks having topology of $\begin{array}{c} \dots \\ \diagup \dots \diagdown \end{array}$ in (92), as well as from the internal such block and from the whole diagram in (93) are performed. These transformations do not change the weight coefficients $\left(a_4^{(l)}\right)_{i_1 i_2 j_1 j_2}$ of the vertices of order $\mathcal{O}(\varepsilon^3)$, but only those of $\begin{array}{c} \diagup \dots \diagdown \\ \diagdown \dots \diagup \end{array}$, i. e., $\left(a_4^{(1)}\right)_{jl} \rightarrow (A_4)_{jl}$, due to the terms on the right hand side of (94) and (95) with factors $\text{0} \begin{array}{c} \dots \\ \diagup \dots \diagdown \end{array}$ and $\text{0} \begin{array}{c} \dots \\ \diagdown \dots \diagup \end{array}$. Note, however, that the latter ones are vanishing unless equal wave-vector-intervals are related to the coupling

lines in these graphs. Based on (94) and (95), some of the coefficients $(A_4)_{jl}$ can be calculated relatively easily. In particular, we have

$$(A_4)_{11}(m) = \left(a_4^{(1)}\right)_{11}(m) + \sum_{j=1}^m \left(2 \left(a_4^{(2)}\right)_{11jj}(m) + \left(a_4^{(3)}\right)_{11jj}(m)\right) b_j(m). \quad (96)$$

The coefficient $\left(A_4^{(1)}\right)_{11}(m)$ appears to be finite at $m \rightarrow \infty$, i. e., the divergent terms in (96) cancel. Nevertheless, the weight coefficients $\left(a_4^{(l)}\right)_{1122}(m)$ with $l = 2, 3$ are the same and divergent in both representations. Moreover, one can conclude from the recurrence relation (76) that $\left(a_4^{(1)}\right)_{jj}(m)$ is divergent not only at $j = 1$, but for any given $j \geq 1$. Consequently, $\left(a_4^{(l)}\right)_{11jj}(m)$ also are divergent for any $j \geq 2$ at $m \rightarrow \infty$ according to (79) and (80). Note that the sums of the corresponding diagrams in (92) and (93) are finite for bounded weight

coefficients, as it can be deduced from the estimations of  and  in Sec. 3.3.

These coefficients, however, are unbounded at $m \rightarrow \infty$. The actual divergences of the quartic terms of order $\mathcal{O}(\varepsilon^3)$ cannot totally cancel, since the divergent weight coefficients are related to different and not reducible to each other diagrams.

Using the representation (91) — (93), one can see that the RG flow behaves in an expected way for not too large m . In this case the form with equal decomposition weight coefficients, considered in Sec. 5.2, is valid as a reasonable approximation. It shows that the sums in (91) — (93) are varied only slightly with increasing of m and the contributions of the large- \mathbf{k} tails are small. The terms, created by the diagrams of order $\mathcal{O}(\varepsilon^3)$ are really small corrections for any large but finite m at $\varepsilon \rightarrow 0$. However, as already discussed at the beginning of Sec. 5.3, one needs to perform $m \gg 1/(\varepsilon \ln s)$ RG transformations to approach the fixed point when starting from an arbitrary $u = \mathcal{O}(\varepsilon)$. While it is normally expected that the RG flow should converge to the fixed point at certain critical initial values of the Hamiltonian parameters, it cannot happen here due to the divergence of $\left(a_4^{(l)}\right)_{11jj}(m)$ with $l = 2, 3$ and $j \geq 2$.

It is easy to verify that this behaviour does not change qualitatively depending on that whether we include or do not include factors originating from the renormalization of the parameter c , as well as those rescaling factors, which provide corrections $o(\varepsilon^3)$ in the formal ε -expansion. The diagrams of the order $\mathcal{O}(\varepsilon^3)$ can be calculated in four dimensions instead of $4 - \varepsilon$ dimensions. In this case (85) is replaced by

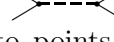
$$\mathcal{Q}(m) = \frac{9}{16} u_{min}^2 \left(\frac{c(m)}{c_{max}}\right)^2 \frac{K_4 \ln s}{c^2(m-1)} \times \frac{s^{2m(\varepsilon-\eta)} - s^{2\varepsilon-2\eta}}{s^{2\varepsilon-2\eta} - 1}, \quad (97)$$

giving rise to an even faster divergence of the Hamiltonian parameters at $m \rightarrow \infty$ and qualitatively the same instability of the RG flow, as discussed before.

Another point is that, at each RGT, we have made certain truncation of the diagram series. By such a method, the omitted terms depend on the specific representation of the diagrams. In our case, the quartic terms are represented by (64), the vertices with more external lines being left in their original form without any subtractions. Our choice is straightforward and quite natural, as it provides certain algorithm of truncation at any desired order of the expansion. In a well defined and reliable perturbation theory with small expansion parameter, the results of truncated series always should be reasonable, if the expansion parameter tends to zero. Our calculations show that this criterion is not satisfied in the ε -expansion.

The divergence of the weight coefficients can be avoided in the calculations up to the order of ε^3 by truncating (at each RGT) the diagram series represented as (92) and (93). A distinguishing feature of the latter representation is that these diagrams converge in four dimensions at $\zeta \rightarrow \infty$ when wave vectors within $k \in [\Lambda, \Lambda\zeta]$ are related to the internal lines (see Sec. 3.3). However, it is not the general solution of the problem, since the above property does not hold for all higher-order diagrams with such kind of hierarchical subtractions of the zero- \mathbf{k} contributions.

A particular example is the diagram .

The actual method can be easily generalized to the case $n \geq 1$, as discussed in Sec. 4. In fact, the same equations are valid, only the factor $9u(m-1)$ has to be replaced with $(n+8)u(m-1)$ in (75) and in (84). However, the decomposition coefficients in general (at $n \neq 1$) have somewhat different meaning: each of them is a prefactor for a weighted sum (with given combinatorial weight factors dependent only on n and normalized in such a way that their sum is 1 at $n = 1$) over a set of different diagrams, made of vertices  , which yield one of the actually considered graphs when the dashed lines shrink to points. Hence, our previous conclusions regarding the behaviour of the RG flow at $n = 1$ refer also to the case $n \geq 1$.

6 Expansion at a fixed spatial dimension d

Apart from the ε -expansion, we have tested also an alternative approach, where the coupling constant u is considered as an expansion parameter at a fixed spatial dimensionality, i. e., fixed ε . In this sense the discussed here approach is similar in spirit to that widely used for calculations in three dimensions, $d = 3$, as described in [14, 15, 16, 17, 18]. However, this known approach uses the Callan–Symanzik equation instead of the Wilson’s equation (3). Besides, the calculations correspond to $\varepsilon = 1$, in which case the coupling constant u is not really a small expansion parameter. To the contrary, we consider a fixed but small ε . It allows, at least formally, to treat u as a small parameter due to the smallness of its fixed-point value.

First, one has to note that all the equations of Sec. 5.4 are valid in this case, except only (97), since ε now is fixed and therefore all the integrals have to be evaluated in $4 - \varepsilon$ dimensions. Because of the same reason, all the rescaling factors of the kind s^ε have to be retained in their original form without the expansion in powers of ε . These requirements are satisfied in the mentioned equations. It leads to the conclusion that the instability of the RG flow due to the divergence of the Hamiltonian parameters of the order $\mathcal{O}(u^3)$ (which are the same as those of the order $\mathcal{O}(\varepsilon^3)$ in the ε -expansion) takes place in this case too.

Following the approach of [14, 15, 16, 17, 18], the critical exponents should be expanded in powers of the coupling constant, estimating their universal values at $u = u^*$. Therefore, the correction factors like $s^{-\eta}$ can be omitted in the first approximation, since one finds that $\eta = \mathcal{O}(u^2)$. Using this idea, and following the calculations in Sec. 3.1, we determine the fixed-point values of u and r in the lowest order of the theory, i. e., \tilde{u}^* and \tilde{r}^* , as

$$\tilde{u}^* = \frac{c^2 \Lambda^\varepsilon}{K_d s^\varepsilon} \frac{2}{n+8} \varepsilon, \quad (98)$$

$$\tilde{r}^* = -\frac{s^2 - s^\varepsilon}{s^{2+\varepsilon} - s^\varepsilon} \frac{c \Lambda^2}{2 - \varepsilon} \frac{n+2}{n+8} \varepsilon. \quad (99)$$

These values are obtained as the fixed-point solutions of (21) and (22), retaining the relevant terms without their expansion in powers of ε . In this case the terms up to the lowest-order

diagrams,  in (21) and  in (22), have been included.

As we see, the fixed-point values depend on the scale parameter s , thus pointing to an internal inconsistency of this method. It is in contrast to the results of the ε -expansion, where such a problem was not detected.

7 Discussion

There are a lot of perturbative RG studies of the φ^4 model made in the past (see [2, 3, 4, 19] for a review). They can be classified as approximative treatments of the perturbation theory in view of our analysis, since a set of apparently irrelevant terms is neglected. Although a perturbative RG approach to critical phenomena never could be considered as a rigorous method, it is, nevertheless, possible to calculate exactly the perturbation terms and to take them into account in a systematic way. In particular, we find that there are many different terms to be included in the renormalized Hamiltonian up to the order of ε^3 , and these terms are relevant in the sense that they do not vanish when repeating the RG transformation unlimitedly many ($m \rightarrow \infty$) times. To the contrary, one usually finds that only few terms, i. e., those included already in the initial Hamiltonian (2) are relevant. A confusion about this apparently is caused by the fact that in the usual (nonrigorous) treatments one looks for the behaviour of individual terms and finds that most of them are shrinking in the renormalization procedure. It, however, is not a rigorous and even not a valid argument, since the $H^{(2m)}$ parts of (62) (as well as any part of $H^{(2m)}$ represented as a sum over diagrams of certain topology) result from many such individual terms, summing up to yield relevant contributions.

The results of perturbative calculations up to the order of ε^5 are reported in literature. These, however, are based on the Callan–Symanzik equation, but not on the Wilson’s equation (3). The Callan–Symanzik equation, in fact, represents a scaling property for the Hamiltonian of the form (2). The approach, thus, relies on the assumption that all the relevant terms are included in the initial Hamiltonian, only the existing here coupling constants being renormalized. This assumption is not supported by our analysis: the perturbative renormalization based on first principles (i. e., avoiding such assumptions via using (3)) produces additional relevant terms. Moreover, their existence is seen already from our calculations up to the order of ε^2 (see Sec. 3), which are absolutely unproblematic from a formal point of view.

The most challenging and interesting result of our study is the instability, i. e., divergence of the perturbative RG flow reported in Sec. 5.4. It shows that the predictions of the perturbative RG theory are not reliable, as regards the asymptotic behaviour of the RG flow and the related estimations of the critical exponents. It can explain the problems with interpretation of the experimental data in liquid helium extremely close to the critical point, discussed in [20, 21].

8 Conclusions

1. A diagrammatic formulation of the perturbative renormalization has been provided (Sec. 2), which makes calculations of perturbation terms straightforward and transparent, avoiding any intermediate approximations.
2. The RG flow equations, including all terms up to the order of ε^2 , have been considered. The tests of the expected properties, such as the semigroup property and the existence of an independent of the scale parameter s fixed point, have been performed. These properties are satisfied up to this order of the ε -expansion (Sec. 3). However, similar tests applied

to an alternative approach, where ε is fixed and the coupling constant u is an expansion parameter, reveal an internal inconsistency (Sec. 6).

3. A truncation scheme has been considered, exactly calculating the perturbation terms and omitting the diagrams of higher than $\mathcal{O}(\varepsilon^3)$ orders. It has been shown that the RG flow in this case behaves reasonably only at the initial stage of the renormalization and never converges to the fixed point (Sec. 5.4). The significance of this fact, as well as of other our results (regarding the relevance or irrelevance of various terms in the renormalized Hamiltonian) has been discussed in Sec. 7.

References

- [1] K. G. Wilson, M. E. Fisher, Phys. Rev. Lett. **28**, 240 (1972)
- [2] Shang-Keng Ma, Modern Theory of Critical Phenomena, W.A. Benjamin, Inc., New York, 1976
- [3] J. Zinn-Justin, Quantum Field Theory and Critical Phenomena, Clarendon Press, Oxford, 1996
- [4] H. Kleinert, V. Schulte-Frohlinde, Critical properties of ϕ^4 theories, World Scientific (2001)
- [5] C. G. Callan, Phys. Rev. D **2**, 1541 (1970)
- [6] K. Symanzik, Commun. math. Phys. **18**, 227 (1970)
- [7] K. Symanzik, Commun. math. Phys. **23**, 49 (1971)
- [8] B. Delamotte, Am. J. Phys. **72**, 170 (2004)
- [9] D. Brydges, J. Dimock, T. R. Hurd, Commun. Math. Phys. **198**, 111 (1998).
- [10] T. Koma, H. Tasaki, Phys. Rev. Lett. **74**, 3916 (1995).
- [11] J. Kaupužs, Int. J. Mod. Phys. C **16**, 1121 (2005)
- [12] J. Kaupužs, Ann. Phys. (Leipzig) **10**, 299 (2001)
- [13] T. Hara, private communication
- [14] G. Parisi, Cargèse Lectures 1973, published in J. Stat. Phys. **23**, 49 (1980)
- [15] E. Brézin, J. C. Le Guillou, J. Zinn-Justin, in *Phase Transitions and Critical Phenomena*, edited by C. Domb, and M. S. Green (Academic, New York, 1976), Vol. 6.
- [16] J. C. Le Guillou, J. Zinn-Justin, Phys. Rev. Lett. **39**, 95 (1977)
- [17] G. A. Baker, B. G. Nickel, M. S. Green, D. I. Meiron, Phys. Rev. Lett., **36**, 1351 (1976)
- [18] G. A. Baker, B. G. Nickel, D. I. Meiron, Phys. Rev. B, **17**, 1365 (1978)
- [19] A. Pelissetto, E. Vicari, Physics Reports **368**, 549 (2002)
- [20] L. S. Goldner, N. Mulders, G. Ahlers, Journal of Low Temperature Physics **93**, 131 (1993)
- [21] J. Kaupužs, Eur. Phys. J. B **45**, 459 (2005)